MACH REFLECTION AND EXPANSION OF TWO-DIMENSIONAL DISPERSIVE SHOCK WAVES: SUPPLEMENTARY MATERIAL

G. Biondini, A. Bivolcic and M. A. Hoefer

August 14, 2025

Here we present further simulation results and relevant background material, as well as various photographs showing observed two-dimensional wave patterns similar to those discussed in the main text.

Invariances of the KP equation. The KP equation possesses a number of physical symmetries, including spatial and temporal translations, scaling, Galilean and "pseudo-rotation", which we take advantage of in this work. Explicitly, if $u(x,y,t)$ is any solution of Eq. (1), then so is $\tilde{u}(x,y,t)$, with

$$\tilde{u}(x,y,t) = a^2 u(ax, a^2 y, a^3 t), \tag{S1a}$$
$$\tilde{u}(x,y,t) = a + u(x-at, y, t), \tag{S1b}$$
$$\tilde{u}(x,y,t) = u(x+ay-a^2 t, y-2at, t), \tag{S1c}$$

for any $a \in \mathbb{R}$, with Eqs. (S1a), (S1b) and (S1c) corresponding to scaling, Galilean and pseudo-rotation transformations, respectively.

Cylindrical KdV reduction of the KP equation. The KP equation admits a self-consistent reduction to the so-called cylindrical KdV equation, namely the (1+1)-dimensional evolution equation [22, 61]

$$u_t + 6uu_\xi + u_{\xi\xi\xi} + d(t)\,u = 0\,. \tag{S2}$$

This reduction is obtained when solutions of Eq. (1) do not depend seprately on x and y, but only on the similarity variable

$$\xi(x,y,t) = x + d(t)y^2\,, \tag{S3a}$$

with

$$d(t) = d_o/(2+4t)\,, \tag{S3b}$$

and where d_o is a constant. Then $u(\xi,t)$ satisfies the cylindrical KdV equation (S2). In the main text, $p(t) = d_o/d(t)$ is referred to as the parabolic curvature coefficient.

Cnoidal waves of the KP equation and characterization of oblique DSWs. The oblique DSWs of the KP equation can be accurately described as a slow spatio-temporal modulation of the periodic traveling wave solutions of the KP equation. In turn, the cnoidal-wave traveling wave solutions of Eq. (1) are conveniently expressed in terms of the parameters r_1, r_2, r_3 as (e.g., see [61])

$$u(x,y,t) = u_{\min} + b\,\mathrm{cn}^2(Z;m)\,, \tag{S4}$$

where

$$Z(x,y,t) = \sqrt{(r_3-r_1)/6}\,(x+qy-ct-x_o)\,, \tag{S5a}$$
$$u_{\min} = r_1 - r_2 + r_3, \tag{S5b}$$
$$b = 2(r_2-r_1)\,, \tag{S5c}$$
$$c = \frac{1}{3}(r_1+r_2+r_3) + q^2\,, \tag{S5d}$$

where

$$m = (r_2-r_1)/(r_3-r_1) \tag{S5e}$$

is the elliptic parameter, and $\mathrm{cn}(Z;m)$ is the Jacobian elliptic cosine [79]. If r_1, r_2, r_3 and q are constant, Eq. (S4) describes an exact, periodic traveling wave solution of the KP equation with peaks along the straight lines $Z = 2nK(m)$, with n integer, $K(m)$ being the complete elliptic integral of the first kind [79]. As $r_2 \to r_1^+$, $m \to 0$ and Eq. (S4) limits to vanishing-amplitude harmonic oscillations. Conversely, as $r_2 \to r_3^-$, $m \to 1$ and Eq. (S4) limits to the soliton solution in Eq. (2). A slanted DSW is obtained when $r_1, r_2 \& r_3$ are given by a self-similar solution of the Whitham modulation equations for the KP equation [61] and $q = \text{const}$, which generalizes the Gurevich-Pitaevski solution of the Whitham modulation equations for the KdV equation [60]. At the rightmost, leading edge of the DSW, $m \to 1$, and the solution limits to a line soliton with amplitude 2Δ, where $\Delta = u_{\max} - u_{\min}$ is the initial jump height. Conversely, at the leftmost, trailing edge of the DSW, $m \to 0$, and the solution limits to oscillations with vanishingly small amplitude. All these solutions can also be obtained as generalizations of y-independent solutions (i.e., solutions of the KdV equation) through the so-called "pseudo-rotation" symmetry of the KP equation (see [61, 80] and the paragraph above).

Dynamics of supercritical type I wedges. Figure S1 shows the temporal evolution of a supercritical type I wedge. The results should be compared to Fig. 1 in the main text, which shows the evolution of a subcritical type I wedge. Although the dynamics in the two cases is qualitatively similar, important quantitative difference exist. Namely, in the supercritical case

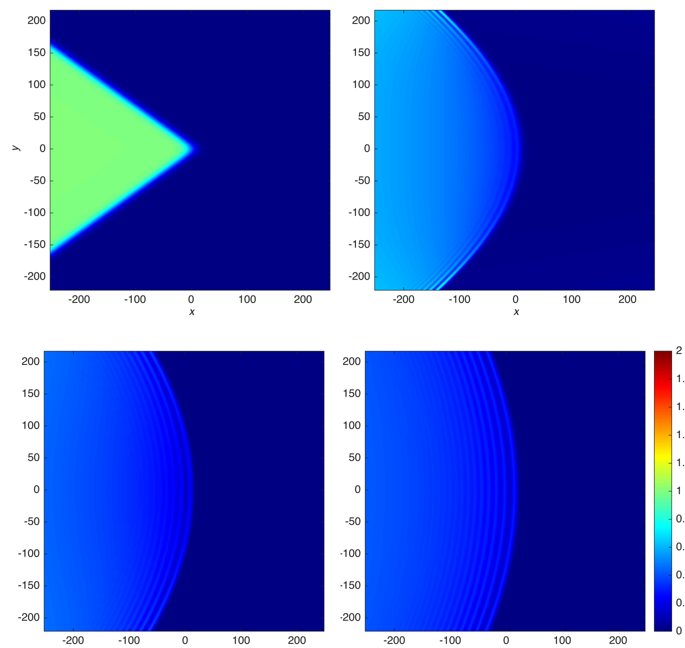

FIG. S1. Same as Fig. 1 in the main text, but for a supercritical type I wedge with $q_o = 1.6$. Note how the amplitude of oscillations near $y = 0$ and the corresponding propagation speed are much smaller compared to those in Fig. 1.

the solution approaches a curved DSW of cylindrical KdV, and amplitude of the oscillations near $y = 0$ correspondingly tends to zero as $t \to \infty$, as discussed in the main text.

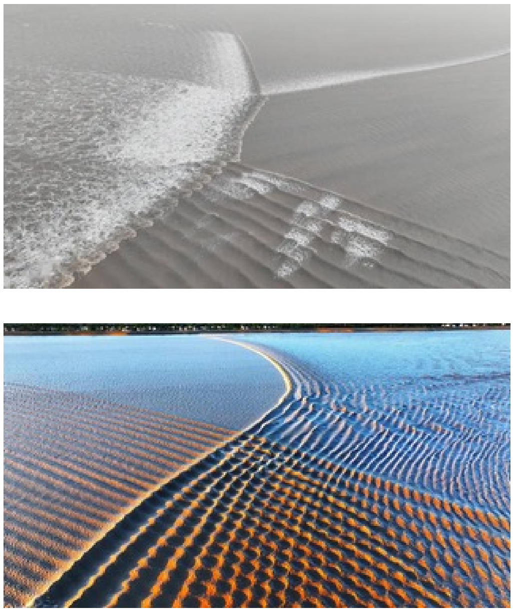

FIG. S2. Two-dimensional undular bore phenomena produced by the Qiantang river tide. Top: From [S1]. Bottom: From [S2].

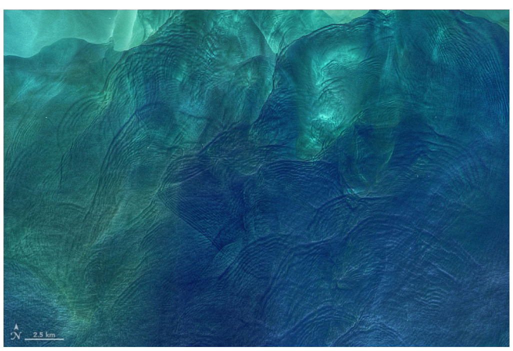

FIG. S3. Interactions between two-dimensional dispersive shock waves in the Andaman sea. From [S3].

FIG. S4. Curved undular bore produced near the mouth of the Araguari river in Brazil. From [S4].

Field observations of multi-dimensional DSWs. Recall that the KP equation (1) is a universal model for weakly nonlinear and two-dimensional shallow/internal water gravity waves. Figure S2 shows the interaction patterns generated by two-dimensional dispersive shock waves in the Qiantang river tide [S2a,S2b]. Note the similarity between these interaction patterns and those in Figs. 2 and 3 in the main text. Note also Fig. S3, which shows what appear to be interactions between two-dimensional dispersive shockd of internal waves in the Andaman sea [S3].

We also point out that the long-time behavior produced by type I wedges appears to be quite common, see for example Fig. S4, which shows the curved undular bore produced near the mouth of the Araguari river in Brazil [S4].

Boundaries between different asymptotic regimes in type II wedges. To further clarify the differences between the asymptotic regimes produced by subcritical and supercritical type II wedges, Fig. S5 shows the boundaries between regions with different asymptotic behavior corresponding to the solutions shown in Figs. 2 and 3 in the main text. The red lines are the leading-edge solitons of the oblique DSWs, the orange line is the leading-edge soliton of the stem DSW, and the blue curves are the boundaries between DSWs and regions of modulated multiphase oscillations. For illustrative purposes, Fig. S6 shows three-dimensional surface plots of the same solutions.

Two-soliton solutions of the KP equation. The KP equation admits a large family of multi-soliton solutions, which have been studied extensively [54–57]. These solutions can be efficiently expressed as

$$u(x,y,t) = 12\,\frac{\partial^2}{\partial x^2}\left[\log\tau(x,y,t)\right], \tag{S6a}$$

$$\tau(x,y,t) = \mathrm{Wr}(f_1,\dots,f_N), \tag{S6b}$$

$$f_n(x,y,t) = \sum_{m=1}^{M} A_{n,m}\,e^{\theta_m(x,y,t)}, \tag{S6c}$$

$$\theta_m(x,y,t) = K_m x + \sqrt{3}\,K_m^2 y - 4K_m^3 t + \theta_{m,0}\,. \tag{S6d}$$

The above solution is uniquely determined by the "phase pa-

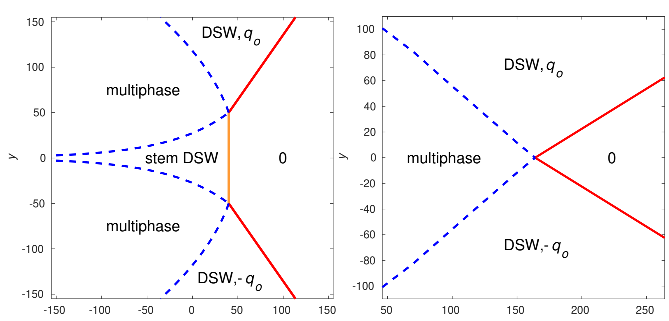

FIG. S5. Boundaries between regions with different type of behavior for solutions produced by subcritical (left) and supercritical (right) type II wedges corresponding to Figs. 2 and 3 in the main text. Red lines: the leading-edge solitons of the oblique DSWs. Orange line: the leading-edge soliton of the stem DSW. Blue curves: boundaries between DSWs and regions of modulated multiphase oscillations.

Table S1: Photograph sources for Figs. [S2–S4]

[S2a] https://www.sohu.com/a/584397607_121106832 (2022)
[S2b] http://www.ezhejiang.gov.cn/2024-09/19/c_1023588.htm (2024)
[S3] https://earthobservatory.nasa.gov/images/146256/making-waves-in-the-andaman-sea (2019)
[S4] https://en.wikipedia.org/wiki/Tidal_ bore#/media/File:Undular_ bore_ Araguari_ River-Brazil-USGS-bws00026.jpg (1988)

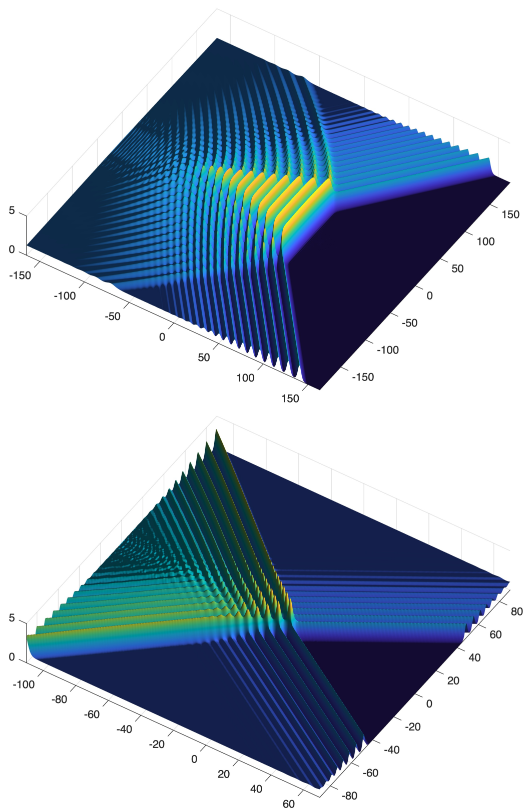

FIG. S6. Three-dimensional surface plots of the solutions in Fig. S5.

rameters" $K_1,\ldots,K_M$ and the coefficient matrix $A=(a_{m,n})$ (together with the translation constants $\theta_{1,0},\ldots,\theta_{M,0}$). Without loss of generality, one can take the phase parameters to be ordered so that $K_1<\cdots<K_M$.

It was shown in [55] that, generically, Eq. (S6a) produces a solution with exactly N asymptotic line solitons as $y\to\infty$ and $M-N$ asymptotic line solitons as $y\to-\infty$. Such solutions are labeled $(M-N,N)$-soliton solutions. The amplitude and slope of each asymptotic line soliton are completely determined by the phase parameters $K_1,\ldots,K_M$, with the precise arrangement depending on the coefficient matrix A. The simplest nontrivial case is obtained when $N=1$ and $M=2$, in which case one recovers the soliton solution (2) with $\bar{u}=0$. Let us label the two phase parameters as K_- and K_+ in this case. The amplitude and slope parameters a and q are given by

$$a=3(K_+-K_-)^2\,,\qquad q=\sqrt{3}\,(K_++K_-)\,. \tag{S7a}$$

Conversely, given a&q, from Eq. (S7a) one obtains $K_\pm$ as

$$K_-=(q-\sqrt{a})/(2\sqrt{3})\qquad K_+=(q+\sqrt{a})/(2\sqrt{3})\,. \tag{S7b}$$

Suppose that one wants to construct a two-soliton solution consisting of two line solitons with amplitude and slope parameters (a_1,q_1) and (a_2,q_2). The resulting two-soliton solution differs depending on the specific values of the soliton parameters. In particular, there are three inequivalent classes of two-soliton solutions [57]. Moreover, as shown in [56], each of these three cases corresponds to a different kind of soliton interaction. Specifically, one can obtain:

(i) An *ordinary* soliton interaction, if and only if $\sqrt{a_1}+\sqrt{a_2}<|q_1-q_2|$, which are associated with the coefficient matrix

$$A_{\rm ord}=\begin{pmatrix}1&1&0&0\\0&0&1&1\end{pmatrix}. \tag{S8a}$$

(ii) A *resonant* soliton interaction, if and only if $|\sqrt{a_1}-\sqrt{a_2}|<|q_1-q_2|<\sqrt{a_1}+\sqrt{a_2}$, which are associated with the coefficient matrix

$$A_{\rm res}=\begin{pmatrix}1&0&-1&-1\\0&1&a_2&a_1\end{pmatrix}, \tag{S8b}$$

with $a_2>a_1>0$.

(iii) An *asymmetric* soliton interaction, if and only if $|q_1-q_2|<|\sqrt{a_1}-\sqrt{a_2}|$, which are associated with the coefficient matrix

$$A_{\rm asymm}=\begin{pmatrix}1&0&0&-1\\0&1&1&0\end{pmatrix}. \tag{S8c}$$

Now note that the two lead solitons in the oblique DSWs in the main text always have equal amplitude $a_s=2$ as well as equal and opposite slope $\pm q_o$. It is then trivial to see that their interaction will be respectively ordinary or resonant depending on whether $|q_o|>\sqrt{a_s}$ or $|q_o|<\sqrt{a_s}$. Thus, the critical angle $q_{\rm cr}=\sqrt{2}$ that separates subcritical and supercritical wedges is precisely the threshold between resonant and ordinary soliton interactions.

Moreover, by explicitly constructing the exact, ordinary two-soliton solution associated with the soliton amplitudes $a_{1,2}=a_s=2$ and slopes $q_{1,2}=\pm q_o$, and by analytically finding its peak, it is straightforward to obtain the expression for the maximum amplitude given in Eq. (6) in the main text.

Mach reflection and expansion of oblique line solitons. Expansive interactions between two oblique line solitons were studied in [64]. There, it was shown that, for a soliton amplitude a_s, initial slopes $q_o>0$ satisfying $0<q_o<\sqrt{a_s}$ result in a Mach expansion (the so-called strong interaction case), in which a steady, one-dimensional line soliton with reduced amplitude is formed in the region around $y=0$. This central, vertical line soliton smoothly connects to the far-field oblique solitons via curved soliton fronts (cf. Fig. S7). Conversely, values $q_o>\sqrt{a_2}$ (the so-called weak interaction case) result in a regular expansion case, in which no vertical line soliton is formed, and the shape of the front near $y=0$ asymptotes to a solution of the cKdV equation with decaying amplitude.

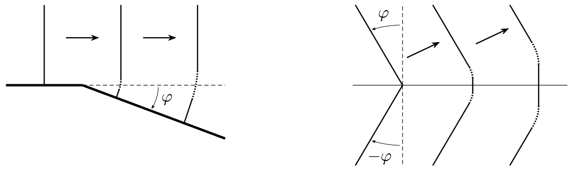

FIG. S7. Right: Mach expansion of an oblique line soliton. Left: the corresponding flow of a vertical line soliton past a subcritical expansive angle. From [64].

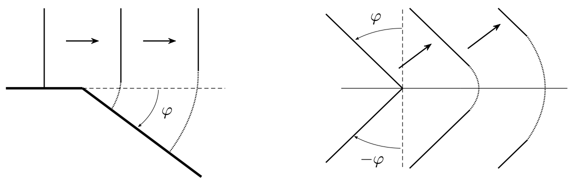

FIG. S8. Right: Regular expansion of an oblique line soliton. Left: the corresponding flow of a vertical line soliton past a supercritical expansive angle. From [64].

FIG. S9. Left: Mach reflection of a vertical line soliton past a subcritical compressive angle. Right: regular reflection past a supercritical angle. From [64].

As shown in Fig. 1 (in which $q_o = 0.4 < \sqrt{2}$) and Fig. S1 (in which $q_o = 1.6 > \sqrt{2}$), and as discussed in the main text, this dichotomy carries over to the expansive interactions between the two oblique DSWs produced by type I wedges. (Recall that the lead soliton in each of the two oblique DSWs has amplitude $a_s = 2$.)

Compressive interactions between two oblique line solitons were studied in [34, 54, 56, 63, 65]. There, it was shown that, for a soliton amplitude a_s, initial slopes $q_o < 0$ satisfying $0 > q_o > -\sqrt{a_s}$ result in a Mach reflection (the strong interaction case), in which a steady, one-dimensional line soliton with higher amplitude is formed in the region around $y = 0$. Conversely, values $q_o < -\sqrt{a_2}$ (the weak interaction case) result in a regular reflection, in which no vertical line soliton is formed (cf. Fig. S9).

As shown in Fig. 2 (in which $q_o = -0.4 > -\sqrt{2}$) and Fig. 3 (in which $q_o = -1.6 < -\sqrt{2}$), and as discussed in the main text, this dichotomy carries over to the compressive interactions between the two oblique DSWs produced by type II wedges.

Numerically computed vertical expansion rate of the stem DSW. Figure S10(left) shows a density plot of the numerically computed maximum of the solution over the x-axis as a function of y and t for a subcritical type II wedge with $q_o = -0.3$, clearly demonstrating the linear vertical expansion of the stem DSW. Figure S10(right) for $q_o < 0$ shows a comparison between the numerically computed transverse expansion rate of the stem DSW in type II wedges for all $-q_{\rm cr} < q_o < 0$ (blue squares) and the analytical prediction from Eq. (4), demonstrating excellent agreement.

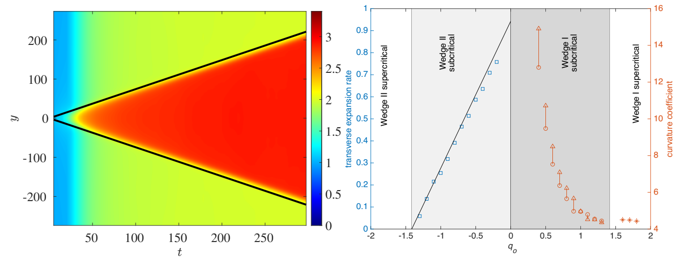

FIG. S10. Left: Density plot of $u(x(t), y, t)$ showing the expansion of the leading-edge vertical soliton stem located at $x = x(t)$ in a subcritical type II wedge with $q_o = -0.3$, plus the analytical prediction from Eq. (4) (black lines). Right, $q_o < 0$: Numerically computed transverse expansion rate dy/dt of the vertical soliton stem in subcritical type II wedges as a function of q_o (blue squares) together with the theoretical prediction from Eq. (4) (black line). Right, $q_o > 0$: Numerically computed parabolic curvature coefficient p_o for supercritical type I wedges (asterisks) and for subcritical type I wedges in the time range $t \in [78, 125]$ (circles) and $t \in [125, 172]$ (triangles) [36].

Numerically computed parabolic curvature coefficient. Figure S10(right) for $q_o > 0$ shows the numerically computed parabolic curvature coefficient for type I wedges. For supercritical wedges ($q_o > q_{\rm cr}$), the measured values (asterisks) are in good agreement with the theoretically predicted value of 4 corresponding to the cKdV reduction. In contrast, for subcritical wedges ($0 < q_o < q_{\rm cr}$), the numerically computed coefficient p_o is itself an increasing function of time, consistent with the fact that the solution near $y = 0$ tends to a constant-amplitude stem DSW.

Further discussion. We should point that multi-phase regions also arise in 1D interacting DSWs (e.g., the KdV equation). A fundamental difference, however, is that in the 1D case the multi-phase regions are eventually extinguished [81], in constrast to the present case, in which these regions expand in time. Also notable is that the slope of each oblique DSW for supercritical type I wedges changes as a result of the interaction with the other one, reminiscent of what happens for 1D and 2D soliton gases [82].

We also point out that the full, analytical characterization of the 2D solutions presented in this work is expected to be challenging because the theory for (2+1)-dimensional systems of conservation laws [83] is still not as well developed. To quantitatively describe the modulated multi-phase regions, one will need multi-phase KP-Whitham equations. Even though such equations can be obtained via the formalism of [84], however, they have never been written down explicitly, let alone used. Degenerate limits of such equations will also be needed to characterize the boundaries between one-phase and multi-phase regions, similarly to [85].